

## TOWARDS AN OPEN-SOURCE, PREPROCESSING FRAMEWORK FOR SIMULATING MATERIAL DEPOSITION FOR A DIRECTED ENERGY DEPOSITION PROCESS

Matthew J. Dantin\*†, William M. Furr\*†, Matthew W. Priddy\*†

\**Department of Mechanical Engineering, Mississippi State University, Mississippi State, MS  
39762, USA*

†*Center for Advanced Vehicular Systems (CAVS), 200 Research Blvd. Starkville, MS 39759*

Keywords: Additive Manufacturing, Directed Energy Deposition, Open-source, G-code, Finite Element Modeling

### **Abstract**

This work focuses on the development of an open-source framework to simulate material deposition for arbitrary geometries with respect to desired process parameters during a directed energy deposition (DED) process. This framework allows the flexibility to define the element activation criteria used in conjunction with Abaqus. A Python script was developed to extract toolpath coordinates from G-code and implement an element activation sequence that is unique to a specific CAD drawing. This is important for simulating the additive manufacturing construction of complex geometries because the thermal history of the component is dependent on laser path, which has a significant effect on residual stresses and distortion. The results of varying the element activation criteria are compared with simulated temperature profiles.

### **Introduction**

Additive manufacturing (AM) is a process for creating near-net shape parts on a layer-by-layer basis, directly from a computer aided design (CAD) model. Many of the metallic AM processes consist of a moving heat source (e.g., laser, electric arc, or electron beam) and material deposition using either extruded wire or powder. There are two main categories of AM processes for producing metal components: (i) powder bed fusion (PBF) and (ii) directed energy deposition (DED). PBF is an AM process that uses a bed of powder, which is compacted by a mechanical spreader, followed by selective melting of regions of the powder bed by a laser or electron beam. DED is an AM process characterized by having a high powered laser that is coaxial with either wire fed or blown powder deposition [1]. DED covers processes such as Laser Engineered Net Shaping (LENS) and direct metal deposition (DMD). A schematic of the DED process is shown in Figure 1. This schematic is specific to the Optomec LENS at the Center for Advanced Vehicular Systems (CAVS) at Mississippi State University [2]. Capabilities of this setup include advanced thermal imaging via a dual wave pyrometer that is mounted coaxial with the laser heat source. Additionally, an infrared camera is mounted inside the build chamber to monitor the side temperature profile of the build. In-situ process monitoring during AM builds is a tool that can be used both by experimental and computational researchers to improve AM across multiple sectors including aerospace, biomedical, chemical, automotive, and defense [3].

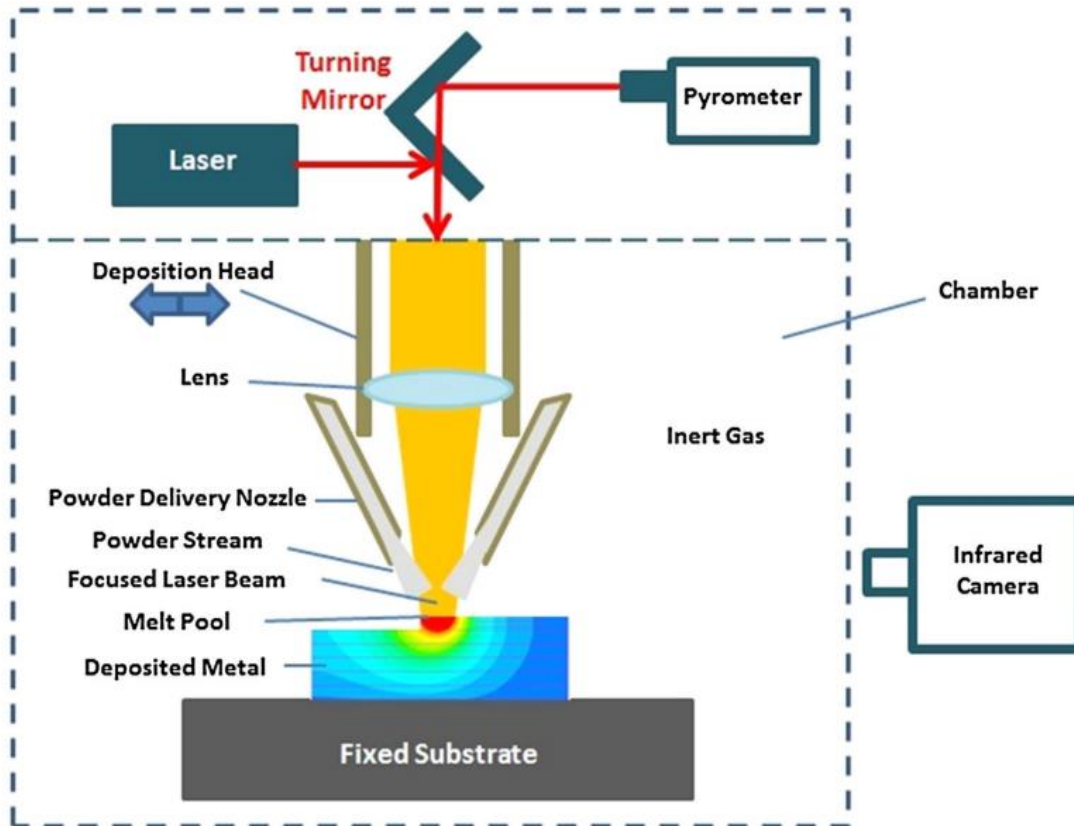


Figure 1: The directed energy deposition process [2].

AM offers a reduction in processing and tooling steps for part production, but often requires post-manufacturing processes such as heat treatment and machining to reduce defects and residual stresses [4]. The two major types of defects present in AM parts are distortion and porosity. Workpiece distortion can be primarily attributed to the buildup of thermally induced residual stresses during AM. Residual stresses in AM parts are generally not desirable because they can negatively impact the maximum load a part can reliably withstand, decrease fatigue life, and cause distortion, all of which reduce the quality of the part [2].

Porosity is the presence of voids in a part, and the presence of voids decreases part density, increases anisotropic behavior if voids are non-spherical, and can cause stress concentrations. AM-related porosity can be categorized as intralayer or interlayer. Intralayer porosity occurs within the deposition layer and is characterized by spherical pores, while interlayer porosity is characterized by elongated, irregularly shaped pores [5]. Interlayer porosity is a result of lack of fusion between layers and is the most detrimental type of porosity experienced in laser based AM [6]. The presence of distortion and porosity in a part adversely affects fatigue life and mechanical properties.

Due to the large thermal gradients and localized heating a workpiece experiences, the complex thermal history of AM processes has proven difficult to control and predict. The thermal history of a workpiece is driven by process parameters such as laser power, scanning speed, hatch spacing, and layer height. Additionally, the thermal history affects the resultant microstructure and defect production. Defects and residual stresses present in AM produced parts reinforce the importance of being able to model and simulate these processes [7].

However, modeling a moving heat source with selective material deposition for component geometry is not a trivial process, because most finite element-based software packages focus on applications that have a constant mass and geometry. This is evident in literature, with a majority of modeling efforts focused on modeling a thin wall [1, 8, 9], but other geometries have been modeled including a large component part [10], a specific complex geometry [11], and a cylinder [12]. Prior to the introduction of a material deposition subroutine in Abaqus 2017, two common methods to simulate material deposition in the AM process are quiet and inactive element activation. For quiet element activation, the element is assigned material properties (e.g. stiffness and thermal conductivity) so that it does not affect the analysis. The user subroutine, UMAT, can be used to model quiet element activation in Abaqus, but the process is cumbersome. For inactive element activation, the elements and associated nodes are not included in the analysis until they have been activated [13]. The user subroutine used to model element activation in Abaqus 2017 utilizes inactive element activation.

The purpose of this work is to present a framework that allows for the simulation of a DED process for an arbitrary component geometry for application in a finite element analysis software. To accomplish this, automation of various tasks within the framework is necessary to reduce the time during the pre-processing steps for simple implementation. This framework allows for complete control over simultaneous material deposition and a moving heat source using desired process parameters, such as laser power, scanning speed, hatch spacing, and layer height along with finite element activation criteria. For the purpose of this paper, the framework uses Abaqus 2017 to model a standard automotive oxygen sensor socket, shown in Figure 2. This part was chosen because it incorporates multiple geometrical features of interest including sharp corners, rounded edges, a cylinder, and a raised wall. Because it can be constructed from different grades of steel, the socket can be manufactured with a DED process. The modeled oxygen sensor socket has a ½” drive.

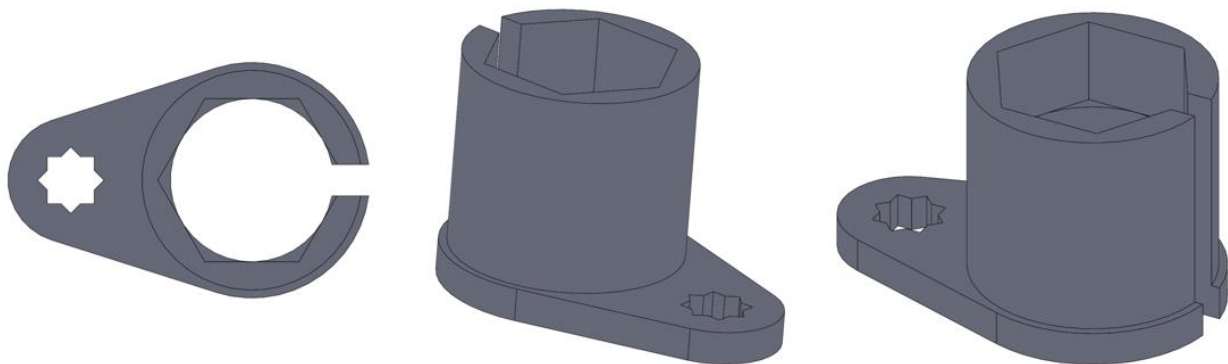


Figure 2: Automotive oxygen sensor socket part geometry.

### **Methodology**

The pre-processing framework for the simulation of material deposition in a DED process is split into three sections: (i) G-code generation from a CAD file using Slic3r [14], (ii) input file generation using a Python script [15], and (iii) implementation into Abaqus 2017 [16]. A flowchart of the pre-processing framework is presented in Figure 3.

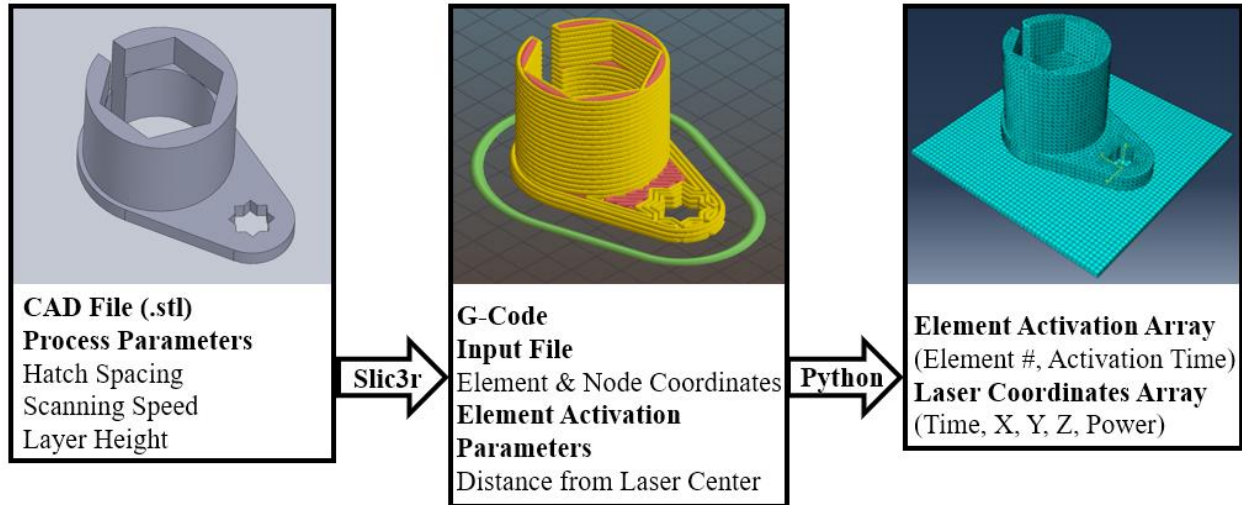


Figure 3: Pre-processing framework flowchart.

The first step in the framework is G-code generation from a 3D CAD file using Slic3r. Types of 3D CAD files that Slic3r can read include: .stl, .obj, .amf, and .pov. For this study, the .stl file was created in SolidWorks [17], but any software capable of producing compatible files such as AutoCAD [18] or Blender [19] can be used. Slic3r is a community-based, open-source program that is used to generate G-code from a CAD file for additive manufacturing [14]. Slic3r was selected because it is open-source, compatible with all G-code languages, and robust. When the CAD file is imported into Slic3r, process parameters such as hatch spacing, laser power, layer height, and scan speed are defined. Once these parameters are set, the material deposition path can be visually verified using Slic3r's automatic visual preview of the material deposition path as shown in the middle image in Figure 3. The preview allows for the material deposition path to be visually inspected and adjusted if necessary. This could provide additional flexibility to the user because of the ability to study additional tool paths and the effect on the thermal history of the workpiece.

Before moving to the second step, an element/nodal input file containing information about the part's mesh is required. The element/nodal input file contains element numbers and their associated nodal connectivity and node number with x-y-z coordinates from the finite element solver's mesh. The CAD file was imported into Abaqus as a .step file to be meshed. For the oxygen sensor socket, a linear tetrahedral mesh was created containing 31,000 heat transfer elements (DC3D4). This framework is not limited to element type or quantity. To avoid convergence issues, the mesh size and timestep should be selected so that the laser travels a maximum length of one element per timestep. Each deposited layer of material is two elements in height.

The second step in the framework is Abaqus input file generation for implementation in the finite element solver. The purpose of this step is to create two arrays: (i) one containing the x-y-z coordinates of the center of the laser at each user defined timestep to simulate a moving heat source and (ii) element number and activation time to simulate simultaneous material deposition using the user defined activation criteria. The element activation criteria are defined as the specific time increment to activate an element based on the distance from the center of the laser to the element's centroid. Activation criteria may differ and can be adjusted depending on a specific AM process due to different material deposition mechanisms and laser heat source profiles.

The Python script uses the G-code generated in the first step, to create the laser coordinates array, which provides the x-y-z coordinate of the laser at each time increment. Additionally, the Python script uses the element/nodal input file to generate an element centroid array. To generate the element activation array, each element centroid is compared to the laser coordinates at each timestep. An element is considered to be activated at the earliest timestep that satisfies two different requirements. The first activation requirement considers the element's centroid coordinate in the build (z) direction. The element's centroid must fall below the z-coordinate of the top of the current layer to meet the first activation requirement. To meet the second requirement, the distance between the center of the laser and the element centroid,  $dr$ , must be less than or equal to the user defined element activation distance,  $r_{act}$ . A schematic of the element activation criteria is presented in Figure 4.

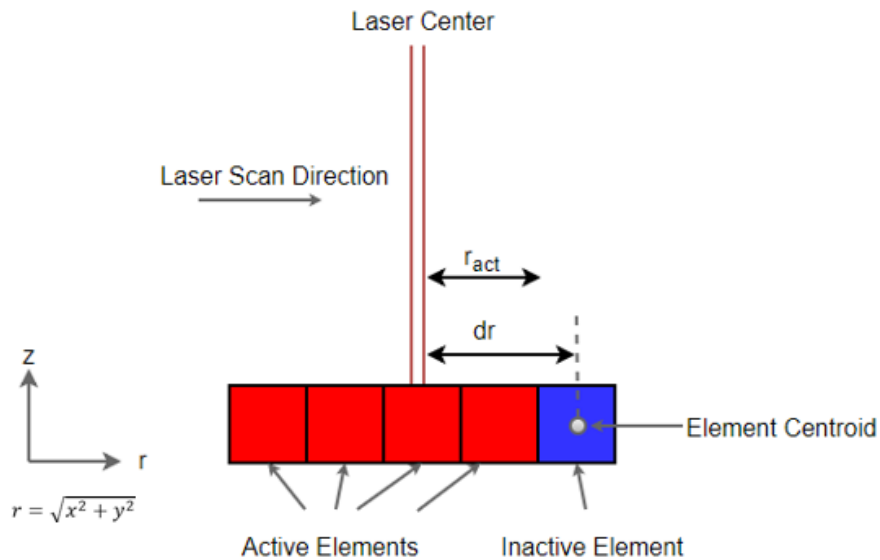


Figure 4: Element activation schematic.

Once the laser coordinates array and the element activation array have been created, the pre-processing framework is ready for implementation. To perform the simulation, two Abaqus user subroutines are needed: DFLUX and UEPActivationVol. The DFLUX subroutine is used to model the laser heat source, and the UEPActivationVol subroutine is used to model material deposition. The laser coordinate array is added to the Abaqus input file as an event series to be called by the DFLUX subroutine, and the element activation array is added to the Abaqus input file as a parameter table to be called by the UEPActivationVol subroutine.

### Results/Discussion

Using the pre-processing framework, two simulations were set up and successfully run modeling the DED process. Once the CAD file, Abaqus input file containing node and element information, and G-code is generated, the Python script takes a few minutes total to run depending on the size of the model. All of this can be performed on a desktop computer with minimal input from the user once the CAD file and element/nodal input file have been created. Although there is room for improvement, this framework is set up so that multiple input files can be generated using different process parameters. The first simulation used the automotive oxygen sensor socket while the second modeled a single layer thin wall.



Each simulation used a Gaussian laser heat source, Ti-6Al-4V as the material, 0.001 s for the timestep, 0.508 mm for the hatch spacing and layer height, and 12.7 mm/s as the scan speed. Temperature dependent properties including density, thermal conductivity, and specific heat were applied to the material model. An emissivity value of 0.54 was used to account for radiation. Additionally, a forced convection boundary condition was applied to the workpiece, and a free convection boundary condition was applied to the substrate to account for the argon shielding gas. The oxygen sensor socket used 31,000 linear tetrahedral heat transfer elements (DC3D4) while the thin wall used 48,000 quadratic brick heat transfer elements (DC3D20). Images showcasing material deposition and temperature field for the oxygen sensor socket simulation at various stages in the process are shown in Figure 5 and Figure 6.

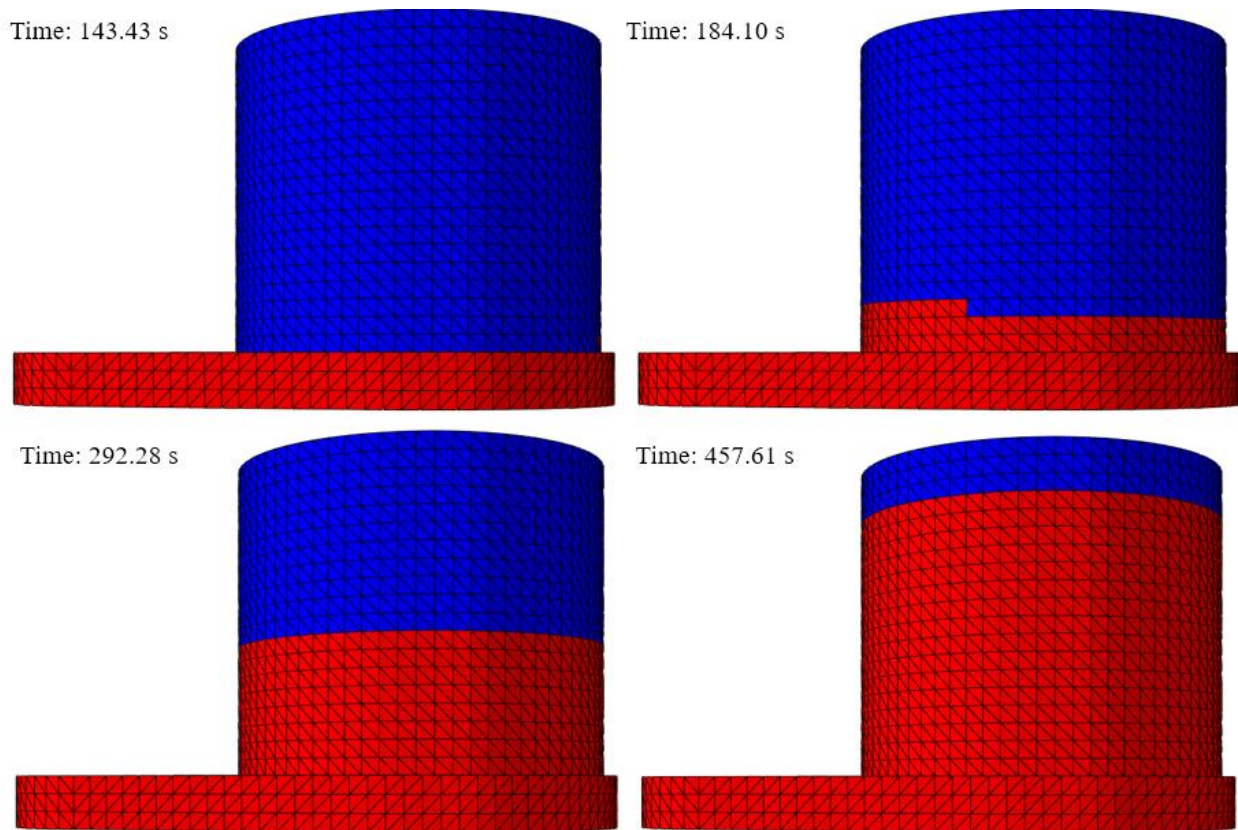


Figure 5: Material deposition simulation images at various time steps. Red elements indicate material deposition and blue elements indicate inactive elements.

The change in the temperature field over time is expected. The base of the socket cools quickly as the simulation progresses as shown in the top two images. This can be partially attributed to heat lost through the substrate due to conduction. However, as shown in the bottom two images, the socket does not cool as quickly as the build progresses away from the substrate. Each layer in the socket head requires less time for material deposition, thus decreasing the amount of cooldown time and increasing temperature buildup.

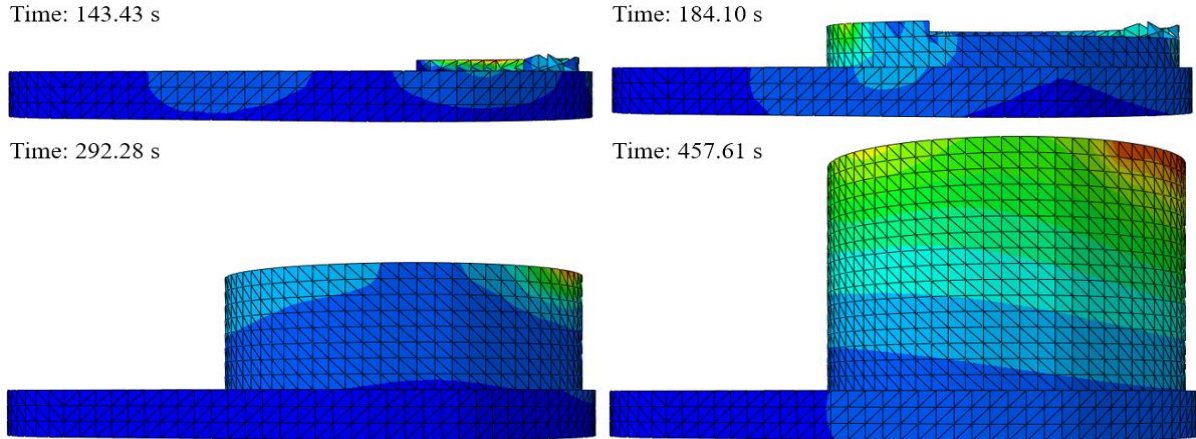


Figure 6: Oxygen sensor socket simulated temperature profile at various time steps.

Upon successful implementation of the pre-processing material deposition framework, the significance of the effect of varying the element activation criteria on the temperature profile of a part was examined. To simplify this comparison, the first layer of a thin wall was modeled using the same process parameters for three simulations. For Case 1, the entire layer of material was activated before applying the moving heat source, essentially simulating the moving laser heat source over an already deposited layer. Case 2 used an activation distance of 1.5 mm from the laser, while Case 3 used an activation distance of 1.75 mm. The activation distance used in Case 3 was also used in the oxygen sensor socket simulation.

The temperature profile for each case across the melt pool is plotted in Figure 7. The most noticeable difference in temperature profile can be observed for Case 3, which has higher temperatures in front of the laser and lower temperatures behind the laser compared to Cases 1 and 2. The resultant temperature field around the melt pool for each case is presented in Figure 8. Notable differences observed in Figure 8 include different melt pool sizes and a longer tail in Case 3. The maximum temperature and melt pool diameter for each case are listed in Table 1. The highest temperature and largest melt pool diameter are observed in Case 1. However, the lowest maximum temperature is observed in Case 3, while Case 2 has the smallest melt pool diameter. The difference in maximum temperature between the three cases is less than 1.5%, but the difference in melt pool diameter is 9.49%.

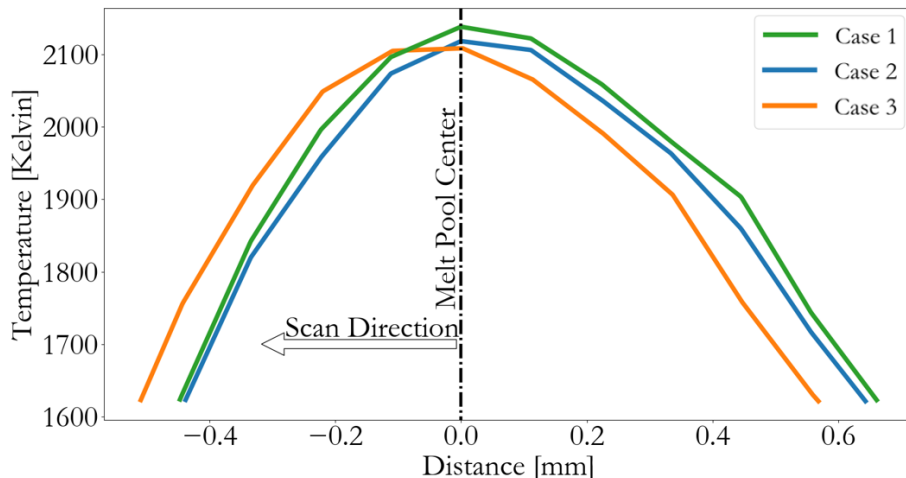


Figure 7: Temperature profile (Kelvin) across the melt pool for each case.



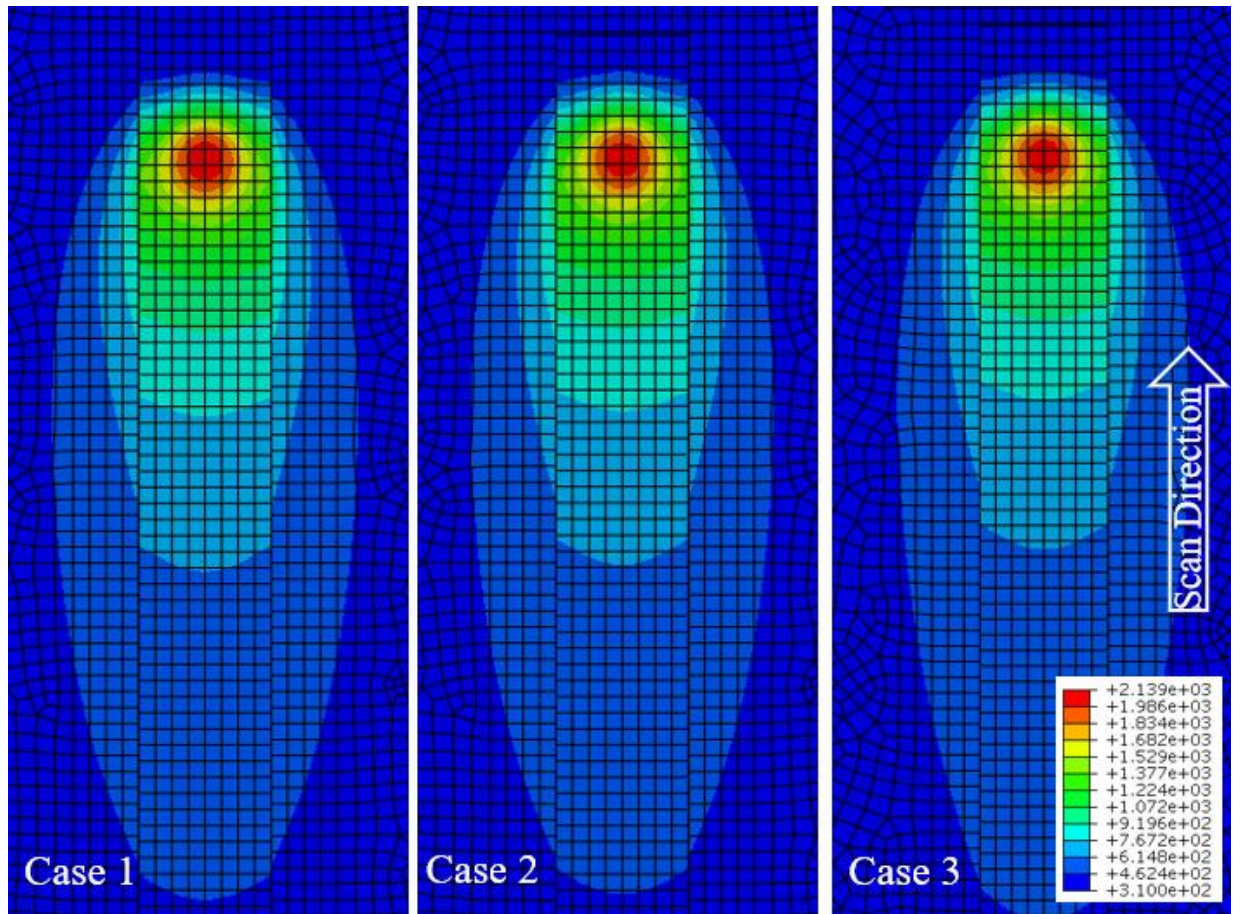


Figure 8: Temperature profiles (Kelvin) for Case 1, Case 2, and Case 3.

Table 1: Maximum temperature and melt pool diameter for each case.

	<b>Maximum Temperature</b>	<b>Melt Pool Diameter</b>
<b>Case 1</b>	2139 K	0.750 mm
<b>Case 2</b>	2119 K	0.682 mm
<b>Case 3</b>	2109 K	0.695 mm

It is evident that using different element activation criteria affects the temperature profile across the melt pool, the maximum temperature, and the melt pool diameter experienced by the workpiece during the DED process. Differences in the temperature field for each case can be attributed to the amount of material available for heat transfer due to conduction, convection, and radiation. These results indicate that the changes in maximum temperature across the three simulations are not as significant as the change in melt pool diameter and temperature profile across the melt pool when considering various element activation criteria.



## **Conclusions**

In this work, a pre-processing framework for the simulation of material deposition for a directed-energy deposition process was presented. The framework was successfully applied to simulate the material deposition of an automotive oxygen sensor socket, and the effect of various element activation criteria on the resultant temperature profile was examined. Due to the variance in temperature profile and maximum temperature observed in each case, further study of how to determine process specific element activation criteria is required. One possible avenue of exploration is the utilization of a high rate camera to measure the distance from laser center to the deposited material. The framework presented in this paper is intended to be further modified to reflect process specific phenomena. The ability to model the material deposition and moving heat source for a directed-energy deposition process for a component geometry is significant because it allows for the simulation of any part. Although many calibration efforts are focused on modeling thin wall geometries, the purpose of AM is the fabrication of complex geometries. This framework allows for the simulation of complex geometries, which can assist with process parameter selection and provide an increase in part quality. Future work will focus on streamlining the pre-processing framework to reduce computation time and resources.

## **Acknowledgements**

Research was sponsored by the Army Research Laboratory and was accomplished under Cooperative Agreement Number W911NF-12-R-0011-03. The views and conclusions contained in this document are those of the authors and should not be interpreted as representing the official policies, either expressed or implied, of the Army Research Laboratory or the U.S. Government. The U.S. Government is authorized to reproduce and distribute reprints for Government purposes notwithstanding any copyright notation herein.

## **References**

- [1] Q. Yang, P. Zhang, L. Cheng, Z. Min, M. Chyu, and A. C. To, "Finite element modeling and validation of thermomechanical behavior of Ti-6Al-4V in directed energy deposition additive manufacturing," *Addit. Manuf.*, vol. 12, pp. 169–177, 2016.
- [2] L. Bian, S. M. Thompson, and N. Shamsaei, "Mechanical Properties and Microstructural Features of Direct Laser-Deposited Ti-6Al-4V," *JOM*, vol. 67, no. 3, pp. 629–638, 2015.
- [3] B. Dutta and F. H. (Sam) Froes, "The Additive Manufacturing (AM) of titanium alloys," *Met. Powder Rep.*, vol. 72, no. 2, pp. 96–106, 2017.
- [4] E. R. Denlinger, J. C. Heigel, and P. Michaleris, "Residual stress and distortion modeling of electron beam direct manufacturing Ti-6Al-4V," *Proc. Inst. Mech. Eng. Part B J. Eng. Manuf.*, vol. 229, no. 10, pp. 1803–1813, 2015.
- [5] L. Wang, P. Pratt, S. Felicelli, H. Kadiri, and P. Wang, "Experimental Analysis of Porosity Formation in Laser-Assisted Powder Deposition Process," *TMS Suppl. Proc. Fabr. Mater. Process. Prop.*, vol. 1, pp. 389–396, 2009.
- [6] C. Qiu, G. A. Ravi, C. Dance, A. Ranson, S. Dilworth, and M. M. Attallah, "Fabrication of large Ti-6Al-4V structures by direct laser deposition," *J. Alloys Compd.*, vol. 629, pp. 351–361, 2015.

- [7] M. M. Francois *et al.*, “Modeling of additive manufacturing processes for metals : Challenges and opportunities,” *Curr. Opin. Solid State Mater. Sci.*, vol. 21, no. 4, pp. 1–9, 2017.
- [8] X. Lu *et al.*, “Finite Element Analysis and Experimental Validation of the Thermomechanical Behavior in Laser Solid Forming of Ti-6Al-4V,” *Addit. Manuf.*, vol. 21, no. February, pp. 30–40, 2018.
- [9] H. Yin, L. Wang, and S. D. Felicelli, “Comparison of Two-Dimensional and Three-Dimensional Thermal Models of the LENS® Process,” *J. Heat Transfer*, vol. 130, no. 10, p. 102101, 2008.
- [10] E. R. Denlinger, J. Irwin, and P. Michaleris, “Thermomechanical Modeling of Additive Manufacturing Large Parts,” *J. Manuf. Sci. Eng.*, vol. 136, no. 6, p. 061007, 2014.
- [11] E. Brusa, R. Sesana, and E. Ossola, “Numerical modeling and testing of mechanical behavior of AM Titanium alloy bracket for aerospace applications,” *Procedia Struct. Integr.*, vol. 5, pp. 753–760, 2017.
- [12] T. M. Rodgers, J. E. Bishop, and J. D. Madison, “Direct Numerical Simulation of Mechanical Response in Synthetic Additively Manufactured Microstructures,” *Model. Simul. Mater. Sci. Eng.*, vol. 26, 2018.
- [13] P. Michaleris, “Modeling metal deposition in heat transfer analyses of additive manufacturing processes,” *Finite Elem. Anal. Des.*, vol. 86, pp. 51–60, 2014.
- [14] A. Ranellucci, “Slic3r Reference Manual 1.2.9.” 2018.
- [15] M. F. Sanner, “Python: a programming language for software integration and development,” *J. Mol. Graph. Model.*, vol. 17, no. 1, pp. 57–61, 1999.
- [16] Hibbett, Karlsson, and Sorensen, *ABAQUS/standard: User’s Manual*, Vol 1. 1998.
- [17] Dassault Systemes, “SolidWorks Reference Manual.” 2018.
- [18] Autodesk, “AutoCAD Reference Manual.” 2018.
- [19] Stichting Blender Foundation, “Blender 2.79 Reference Manual.” Amsterdam, 2018.